River Flow 2022 – Ferreira da Silva et al. (eds)

Direct visualization of hyporheic exchange in an emergent vegetation canopy

S.H. Huang & J.Q. Yang
Department of Civil, Environmental, and Geo- Engineering, University of Minnesota, Minneapolis, USA
Saint Anthony Falls Laboratory, University of Minnesota, Minneapolis, USA

ABSTRACT: Aquatic vegetation has been used to restore streams, stabilize riverbanks, and improve water quality. Field studies show that aquatic vegetation increases the in-stream transient storage in the hyporheic zone. However, the impact of vegetation on hyporheic exchange has not been quantified due to a lack of direct visualization of the three-dimensional (3D) pathway of hyporheic exchange in channels with vegetation. The goal of this study is to quantify hyporheic exchange induced by emergent vegetation through visualization in a laboratory flume. We proposed three probable mechanisms by which emergent vegetation impacts hyporheic exchange. To validate our hypotheses, we developed a refractive index match-based method to directly image the trajectories of fluorescent dye in a channel filled with transparent gravel sediment made from hydrogel beads and translucent acrylic vegetation dowels.

1 INTRODUCTION

Hyporheic zone is commonly referred to as the sediment layer near the surface water-groundwater interface in rivers and streams (Boano et al. 2014, Boulton et al. 1998, Gooseff 2010). The pore fluid in the hyporheic zone and the surface water are constantly exchanging dissolved gases, solutes, nutrients, and pollutants, which controls the biogeochemical cycles and biodiversity of the benthic habitats (Battin et al. 2008, Jones Jr & Holmes 1996, Tonina & Buffington 2009, Wohl 2016) and determines the retention and degradation of contaminants in the streams (Grant et al. 2014, Lewandowski et al. 2011, McCallum et al. 2020). To increase our ability to manage the biogeochemical cycle and fate of contaminants as well as preserve biodiversity in aquatic environments, a fundamental understanding of hyporheic exchange is desired.

Most studies of hyporheic exchange focus on quantifying hyporheic exchange driven by bedforms (Buffington & Tonina 2009, Dudunake et al. 2020, Marion et al. 2002, Packman et al. 2004, Tonina & Buffington 2007), river sinuosity (Boano et al. 2006, Cardenas 2009), and turbulence (Roche et al. 2018, Roche et al. 2019, Rousseau & Ancey 2020, Voermans et al. 2017, Voermans et al. 2018b). Recent field investigations and numerical studies show that the presence of in-channel vegetation increases in-stream transient storage (Ensign & Doyle 2005, Salehin et al. 2003) and induces hyporheic exchange near the vegetation stems (Yuan et al. 2021). However, the impacts of in-channel vegetation on hyporheic exchange have not been systematically characterized.

Here, we hypothesize that vegetation can induce hyporheic exchange within a canopy through three mechanisms. To test these hypotheses, we designed hyporheic visualization experiments in a recirculating flume with refractive index-matched sediment and translucent acrylic dowels.

DOI: 10.1201/9781003323037-95

2 THEORY

We hypothesize that within an emergent vegetation canopy, i.e., with vegetation dowels protruding through the water surface, vegetation impacts hyporheic exchange through the following three mechanisms.

First, we hypothesize that stem-scale pressure gradient generated by vegetation drag (Nepf & Koch 1999) can drive stem-scale hyporheic exchange (Figure 1). This hypothesis is confirmed by a recent Reynolds-averaged Navier-Stoke simulation (Yuan et al. 2021), which shows that stem-scale pressure gradient generated by vegetation can indeed induce hyporheic exchange.

The drag exerted by the vegetation F_D on the surface flow has been expressed as a function of flow velocity and vegetation characteristics (Cheng & Nguyen 2011, Nepf 2012):

$$F_D = \frac{1}{2} a V_{ol,v} C_D \rho_w U^2 \tag{1}$$

Here a is the vegetation frontal area per unit canopy volume (m^{-1}) which can be estimated as $a = nd_v$ for cylindrical vegetation (Yang & Nepf 2018); n is the stem density (stem/m^2); d_v is the diameter of model vegetation stem (m); C_D is the drag coefficient of the vegetation; $V_{ol,v}$ is the volume of the surface water within vegetation canopy (m^3); ρ_w is fluid density (kg/m^3), and U is the spatially-averaged velocity of the surface flow (m/s).

Second, we anticipate that vegetation can increase hyporheic exchange by increasing the total near-bed turbulent kinetic energy. Turbulence has been shown to increase mixing between surface water and the hyporheic zone (Nagaoka & Ohgaki 1990, Vollmer et al. 2002, O'Connor & Hondzo 2008, Voermans et al. 2018b). In an emergent vegetation canopy, the energy extracted from the mean flow due to the vegetation drag can be used to estimate vegetation-generated spatial-averaged turbulent kinetic energy k_{tv} (Tanino & Nepf 2008, Yang et al. 2016):

$$k_{tv} = 1.2\left[C_D \frac{\phi_v}{(1-\phi_v)\pi/2}\right]^{2/3} U^2 \tag{2}$$

Here ϕ_v is the solid fraction of the vegetation. For cylindrical dowels, $\phi_v = \pi a d_v/4$ (Yang & Nepf 2018). One can approximate the total near-bed turbulent kinetic energy k_t as the sum of bed-generated k_{tb} and vegetation-generated k_{tv} that $k_t = k_{tb} + k_{tv}$ (Yang et al. 2016, Yang & Nepf 2018, 2019).

Third, we conjecture that vegetation impacts hyporheic exchange by increasing horizontal velocity of pore fluid within the sediment, because under the same mean flow velocity, vegetation increases the water surface slope and as such increases the streamwise pressure gradient in the sediment. The surface slope S can be calculated from vegetation characteristics and flow velocity based on force balance, i.e., the streamwise pressure gradient driven by surface slope balances the bed friction and vegetation drag:

$$\rho_w g H S = C_f \rho_w U^2 + \frac{1}{2} a \rho_w H C_D U^2 \tag{3}$$

Here g is gravitational acceleration (m/s^2); H is the water depth (m); S is the water surface slopes; C_f is bed drag coefficient; The bed drag coefficient C_f can be estimated as $C_f = (5.75\log(12.1H/k_s'))^{-2}$ in a rough channel with the grain roughness height $k'_s = 6.8d_{50}$ for gravels, i.e., sediment diameter $d_s > 2$ mm (Julien 2010). The streamwise pressure gradient due to surface slope is $dP/dx = \rho_w g S$ with x denoting streamwise distance. Accordingly, the horizontal pore fluid velocity, V_h(m/s), within the sediment can be estimated based on Darcy's law: $V_h = -k/\mu\phi_s \times dP/dx$, with ϕ_s denoting sediment porosity, k denoting the permeability of the sediment bed (m^2), d_s denoting the sediment diameter (m), and μ denoting the dynamic

viscosity (Pa · s). k can be estimated from the Karman-Cozeny relationship: $k = \phi_s^3 d_s^2 / 180(1-\phi_s)^2$ (Voermans et al. 2018a).

In summary, we hypothesize that emergent vegetation may induce hyporheic exchange by increasing stem-scale pressure gradient, near-bed turbulence, and water surface slope within the vegetation canopy. The three mechanisms mentioned above are summarized in Figure 1.

In this study, we first demonstrate that the presence of vegetation increases the hyporheic exchange using dye visualization experiment. Second, we discuss how vegetation impacts the horizontal velocity of pore fluid within the sediment. Note that the exact contribution of each of the above three mechanisms on hyporheic exchange cannot be separated in our current experimental setup.

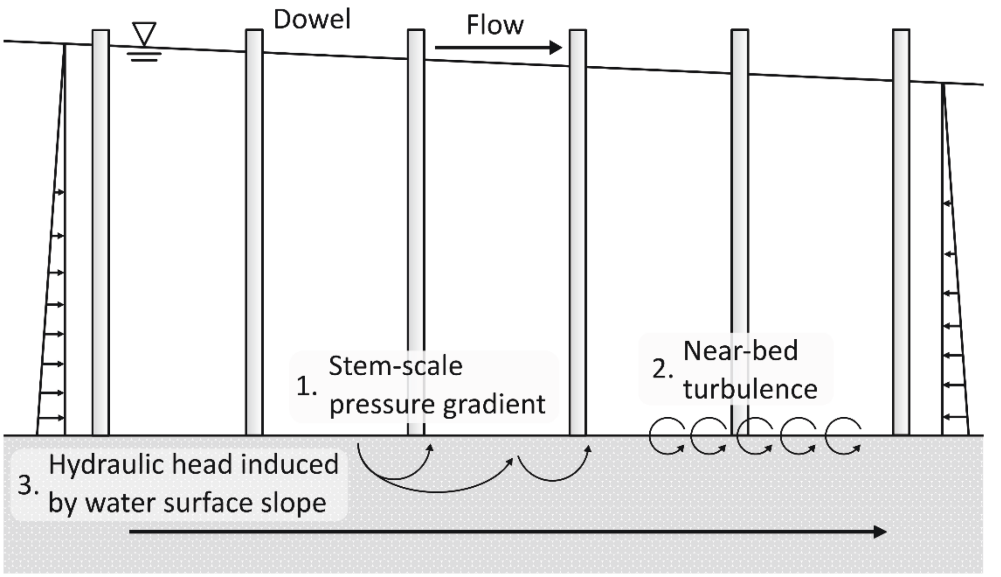

Figure 1. We propose three mechanisms by which emergent vegetation impacts hyporheic exchange within a canopy.

3 METHODOLOGY

A 14 m-long, 0.6 m-wide horizontal race-track flume at the University of Minnesota's St. Anthony Falls Laboratory was used to conduct the dye visualization experiments. The measurements of the experiments were taken on a 150-cm-long by 60-cm-wide straight test section. To model a permeable gravel bed, the transparent hydrogel beads (5.6 ± 0.6 mm in diameter) were filled into the space underneath the test section. The sediment porosity $\phi_s = 0.3$. The characteristic length scale of the pore space $\Lambda = d_s/2m\left(\phi_s^{-m} - 1\right) = 0.4$ mm. Here m is the grain shape parameter. For perfect spherical grains, m = 1.5 (Revil 2002, Revil & Cathles III 1999). We covered the hydrogel beads with a black polyester mesh (4 mm pore size) to keep the beads in place and the sediment bed flat. The method proposed by Ma et al. (2019) was used to make the hydrogel beads.

The translucent and cylindrical acrylic dowels with diameter d_v = 6.4 ± 0.1 mm were used to simulate a rigid vegetation canopy. The dowels were arranged in a staggered array of stem density n = 1514 stem/m^2 and with spanwise center-to-center distance $2ds$ = 2.6 cm on a perforated PVC board placed under the hydrogel beads. The vegetation frontal area per unit canopy volume a is 9.8 m^{-1}. The vegetation solid volume fraction ϕ_v = 0.05 is in the range of typical conditions in marches (Nepf 2012, Yang et al. 2016). Note that the dowels filled the whole sediment depth and protruded through the water surface.

We added fluorescein sodium salt (Sigma-Aldrich F6377) to DI water at 0.002‰ weight ratio to prepare dye solution. In the experiment, the fluorescent dye in the sediment was stimulated by the blue light of a square lamp (30 cm × 30 cm) with blue LED arrays (Figure 2) and emitted green light. The fluorescence was monitored by a downward-looking industrial camera (BFS-U3-16S2C-CS; FLIR Systems, Wilsonville) with a 6 mm focal length lens (ArduCAM, China) and a side-looking Nikon camera (D7500; Nikon, Japan). The intensity of background blue light was reduced by green light filters (FGV9S; Thorlabs, Newton). The fluorescence intensity was linearly proportional to the dye concentration according to calibration tests (Huang & Yang 2022). The experimental setup is shown in Figure 2.

Two types of dye visualization experiments were conducted: dye release experiment and point-injection experiment. For dye release experiment, 1200 mL of fluorescent dye was injected uniformly into a 44 cm × 43 cm sediment area up to 5 cm from the sediment-water interface at quiescent condition. Afterwards, flow was started by a propeller. The time evolution of the fluorescent intensity of the dye in the sediment bed was captured by a downward-looking camera over 17 hours. For point-injection experiments, 5 mL of the dye was injected into the sediment during the flow condition. The migration of the dye plume in the sediment was captured by a downward-looking camera as well as a side-looking camera.

The flow velocities in the test section at various vertical and spanwise locations were measured using a side-looking Acoustic Doppler Velocimeter (Nortek Vectrino, Norway). The water depth in all experiments was 20.0 ± 0.1 cm, and the spatially and temporally-averaged flow velocity was 4 cm/s.

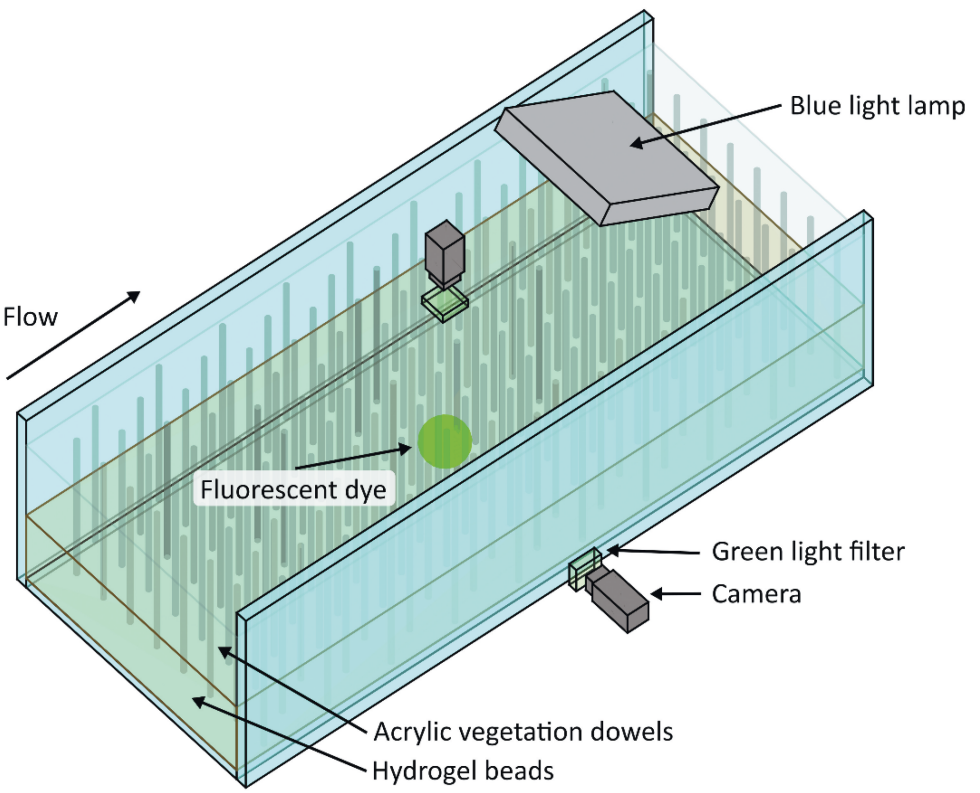

Figure 2. Schematic diagram of the setup of hyporheic exchange visualization experiments.

4 RESULTS AND DISCUSSIONS

First, we investigate the overall effect of the above proposed three mechanism (Figure 1) through dye release experiments with and without vegetation. We tracked the decrease in the average fluorescence intensity of the dye in the sediment over a 22 cm × 17 cm area, which contains several repeated patterns of vegetation dowels (47 dowels in the area) for the case with vegetation. At the same spatially and temporally-averaged flow velocity $U = 4$ cm/s, the decrease in fluorescence intensity was faster in the channel with vegetation than in the non-vegetated channel (Figure 3), indicating that the presence of emergent vegetation increased the rate of hyporheic exchange.

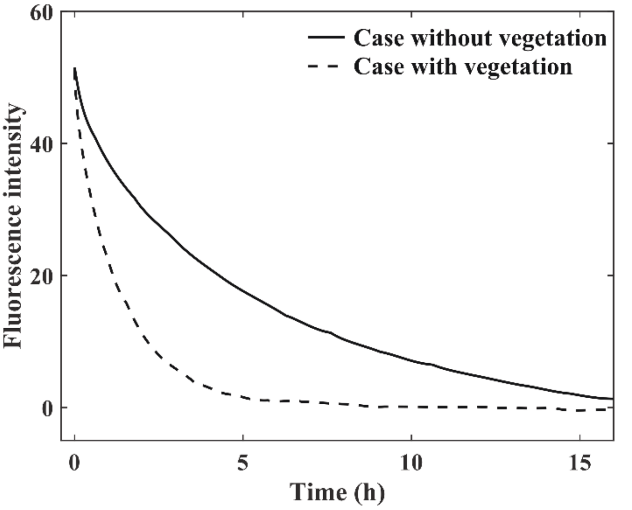

Figure 3. Average fluorescence intensity, which indicates the amount of dye in the sediment, decreased over time due to hyporheic exchange. The spatially-averaged velocity of surface water for both cases is the same, i.e., $U = 4$ cm/s.

Second, we evaluate the impacts of vegetation on the streamwise migration of the dye plume in the sediment (i.e., mechanism 3 in Figure 1) by tracking the trajectories of dye during the point-injection experiments (Figure 4). At the same mean flow velocity of surface water $U = 4$ cm/s, the velocities of the center of dye plume with and without vegetation are $(2.0 \pm 1.0) \times 10^{-2}$ and $(2.5 \pm 0.5) \times 10^{-4}$ cm/s, respectively, suggesting that vegetation increased streamwise flow velocity within the sediment by almost two orders of magnitude. The Reynolds number of the surface flow $Re = UR_h/\nu$ is 4800. Here $R_h = WH/(2H+W)$ is hydraulic radius (m); W is channel width (m), and ν is kinematic viscosity (m^2/s). To calculate the Reynolds number in the sediment Re_s, one should replace R_h with Λ-parameter (Crespy et al. 2007). For cases with and without vegetation, Re_s are 0.07 and 0.001, respectively.

Based on the water surface slope equation (Eq. 3) and Darcy's law, we estimated that at $U = 4$ cm/s the horizontal migration velocities of the pore fluid are 2.5×10^{-2} and 2.3×10^{-4} cm/s for vegetated and non-vegetated channels, respectively. The agreement of our theory and experimental results confirms that vegetation can indeed increase the horizontal velocity of pore fluid in the sediment by orders of magnitude by increasing water surface slope.

Due to the intrinsic complexity of vegetation-flow-sediment interactions, our study cannot distinguish the exact contribution of each mechanism (Figure 1) to the overall hyporheic exchange. Nevertheless, the quantitative measurements here provide quantitative evaluation of the overall impacts of vegetation on hyporheic change and the underlying mechanisms.

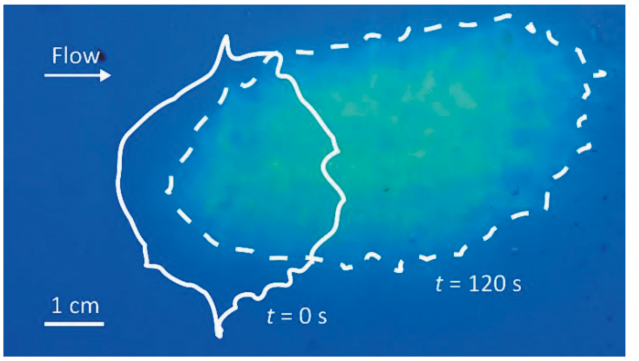

Figure 4. The streamwise migration of dye plume in the sediment bed of a vegetated channel. The dye was injected 8 cm below the sediment-water interface. The region circled by the solid curve indicates the initial location of the injected dye plume. The region circled by the dashed line illustrates the location of the dye plume at t = 120 s.

5 CONCLUSIONS

Here we propose three mechanisms by which emergent vegetation impacts hyporheic exchange within a vegetation canopy, including increasing (1) stem-scale pressure gradient, (2) near-bed turbulence, and (3) water surface slope within the vegetation canopy. We designed dye visualization experiments using transparent hydrogel beads and fluorescent dye to visualize the 3D pathway of hyporheic exchange within the sediment. We show that the presence of the emergent vegetation increases the exchange of fluorescent dye between surface and subsurface flow. We also show that the horizontal migration velocity of the dye plume in the sediment bed is consistent with the fluid velocity driven by the canopy-induced hydraulic gradient. The refractive index match-based method we propose here will enable more thorough investigations of the impacts of aquatic vegetation on hyporheic exchange.

ACKNOWLEDGEMENTS

This work is supported by NSF EAR 2209591.

NOTATION

The symbols used in this paper are as follows:

a = vegetation frontal area per unit canopy volume;
C_D = drag coefficient of the vegetation;
C_f = bed drag coefficient;
d_s = sediment diameter;
ds = half of spanwise center-to-center distance;
d_v = diameter of model vegetation stem;
d_{50} = median sediment diameter;
F_D = drag exerted by the vegetation;
g = gravitational acceleration;
H = water depth;
k = permeability of the sediment bed;
k_s' = grain roughness height;
k_t = total near-bed turbulent kinetic energy;
k_{tb} = bed-generated turbulent kinetic energy;

k_{tv} = vegetation-generated turbulent kinetic energy;
m = grain shape parameter;
n = stem density;
Re = Reynolds number;
Re_s = Reynolds number is the sediment;
R_h = hydraulic radius;
S = water surface slope;
U = the spatially-averaged velocity of the surface flow;
V_h = horizontal pore fluid velocity;
$V_{ol,v}$ = the volume of the surface water within vegetation canopy;
W = channel width;
Λ = characteristic length scale of the pore space;
μ = dynamic viscosity;
v = kinematic viscosity;
ρ_w = fluid density;
ϕ_s = sediment porosity; and
ϕ_v = solid fraction of the vegetation.

REFERENCES

Battin, T. J., Kaplan, L. A., Findlay, S., Hopkinson, C. S., Marti, E., Packman, A. I., Newbold, J. D. & Sabater, F. 2008. Biophysical controls on organic carbon fluxes in fluvial networks. *Nature geoscience* 1(2): 95–100.

Boano, F., Camporeale, C., Revelli, R. & Ridolfi, L. 2006. Sinuosity-driven hyporheic exchange in meandering rivers. *Geophysical Research Letters* 33(18).

Boano, F., Harvey, J. W., Marion, A., Packman, A. I., Revelli, R., Ridolfi, L. & Wörman, A. 2014. Hyporheic flow and transport processes: Mechanisms, models, and biogeochemical implications. *Reviews of Geophysics* 52(4): 603–679.

Boulton, A. J., Findlay, S., Marmonier, P., Stanley, E. H. & Valett, H. M. 1998. The functional significance of the hyporheic zone in streams and rivers. *Annual review of Ecology and systematics* 29(1): 59–81.

Buffington, J. M. & Tonina, D. 2009. Hyporheic exchange in mountain rivers II: Effects of channel morphology on mechanics, scales, and rates of exchange. *Geography Compass* 3(3): 1038–1062.

Cardenas, M. B. 2009. A model for lateral hyporheic flow based on valley slope and channel sinuosity. *Water Resources Research* 45(1).

Cheng, N. S. & Nguyen, H. T. 2011. Hydraulic radius for evaluating resistance induced by simulated emergent vegetation in open-channel flows. *Journal of hydraulic engineering* 137(9): 995–1004.

Crespy, A., Boleve, A. & Revil, A. 2007. Influence of the Dukhin and Reynolds numbers on the apparent zeta potential of granular porous media. *Journal of Colloid and Interface Science* 305(1): 188–194.

Dudunake, T., Tonina, D., Reeder, W. & Monsalve, A. 2020. Local and Reach-Scale Hyporheic Flow Response From Boulder-Induced Geomorphic Changes. *Water Resources Research* 56(10): e2020WR027719.

Ensign, S. H. & Doyle, M. W. 2005. In-channel transient storage and associated nutrient retention: Evidence from experimental manipulations. *Limnology and oceanography* 50(6): 1740–1751.

Gooseff, M. N. 2010. Defining hyporheic zones–advancing our conceptual and operational definitions of where stream water and groundwater meet. *Geography Compass* 4(8): 945–955.

Grant, S. B., Stolzenbach, K., Azizian, M., Stewardson, M. J., Boano, F. & Bardini, L. 2014. First-order contaminant removal in the hyporheic zone of streams: Physical insights from a simple analytical model. *Environmental Science & Technology* 48(19): 11369–11378.

Huang, S. H., & Yang, J. Q. (2022). Impacts of Emergent Vegetation on Hyporheic Exchange. *Geophysical Research Letters* 49(13): e2022GL099095.

Jones Jr, J. B. & Holmes, R. M. 1996. Surface-subsurface interactions in stream ecosystems. *Trends in Ecology & Evolution* 11(6): 239–242.

Julien, P. Y. 2010. *Erosion and sedimentation*. Cambridge: Cambridge university press.

Lewandowski, J., Putschew, A., Schwesig, D., Neumann, C. & Radke, M. 2011. Fate of organic micropollutants in the hyporheic zone of a eutrophic lowland stream: Results of a preliminary field study. *Science of the Total Environment* 409(10): 1824–1835.

Ma, L., Shi, Y., Siemianowski, O., Yuan, B., Egner, T. K., Mirnezami, S. V., Lind, K. R., Ganapathysubramanian, B., Venditti, V. & Cademartiri, L. 2019. Hydrogel-based transparent soils for root phenotyping in vivo. *Proceedings of the National Academy of Sciences* 116(22): 11063–11068.
Marion, A., Bellinello, M., Guymer, I. & Packman, A. 2002. Effect of bed form geometry on the penetration of nonreactive solutes into a streambed. *Water Resources Research* 38(10): 27–1-27-12.
McCallum, J. L., Höhne, A., Schaper, J. L., Shanafield, M., Banks, E. W., Posselt, M., Batelaan, O. & Lewandowski, J. 2020. A numerical stream transport modeling approach including multiple conceptualizations of hyporheic exchange and spatial variability to assess contaminant removal. *Water Resources Research* 56(3): e2019WR024987.
Nagaoka, H. & Ohgaki, S. 1990. Mass transfer mechanism in a porous riverbed. *Water Research* 24(4): 417–425.
Nepf, H. M. 2012. Flow and transport in regions with aquatic vegetation. *Annual Review of Fluid Mechanics* 44: 123–142.
Nepf, H. M. & Koch, E. W. K. 1999. Vertical secondary flows in submersed plant-like arrays. *Limnology and Oceanography* 44(4): 1072–1080.
O'Connor, B. L. & Hondzo, M. 2008. Dissolved oxygen transfer to sediments by sweep and eject motions in aquatic environments. *Limnology and Oceanography* 53(2): 566–578.
Packman, A. I., Salehin, M. & Zaramella, M. 2004. Hyporheic exchange with gravel beds: Basic hydrodynamic interactions and bedform-induced advective flows. *Journal of Hydraulic Engineering* 130(7): 647–656.
Revil, A. 2002. The hydroelectric problem of porous rocks: thermodynamic approach and introduction of a percolation threshold. *Geophysical Journal International* 151(3): 944–949.
Revil, A., & Cathles III, L. M. 1999. Permeability of shaly sands. *Water Resources Research* 35(3): 651–662.
Roche, K., Blois, G., Best, J., Christensen, K., Aubeneau, A. & Packman, A. 2018. Turbulence links momentum and solute exchange in coarse-grained streambeds. *Water Resources Research* 54(5): 3225–3242.
Roche, K. R., Li, A., Bolster, D., Wagner, G. J. & Packman, A. I. 2019. Effects of turbulent hyporheic mixing on reach-scale transport. *Water Resources Research* 55(5): 3780–3795.
Rousseau, G. & Ancey, C. 2020. Scanning PIV of turbulent flows over and through rough porous beds using refractive index matching. *Experiments in Fluids* 61(8): 1–24.
Salehin, M., Packman, A. I. & Wörman, A. 2003. Comparison of transient storage in vegetated and unvegetated reaches of a small agricultural stream in Sweden: seasonal variation and anthropogenic manipulation. *Advances in Water Resources* 26(9): 951–964.
Tanino, Y. & Nepf, H. M. 2008. Lateral dispersion in random cylinder arrays at high Reynolds number. *Journal of Fluid Mechanics* 600: 339–371.
Tonina, D. & Buffington, J. M. 2007. Hyporheic exchange in gravel bed rivers with pool-riffle morphology: Laboratory experiments and three-dimensional modeling. *Water Resources Research* 43(1).
Tonina, D. & Buffington, J. M. 2009. Hyporheic exchange in mountain rivers I: Mechanics and environmental effects. *Geography Compass* 3(3): 1063–1086.
Voermans, J. J., Ghisalberti, M. & Ivey, G. 2017. The variation of flow and turbulence across the sediment–water interface. *Journal of Fluid Mechanics* 824: 413–437.
Voermans, J. J., Ghisalberti, M. & Ivey, G. N. 2018a. A model for mass transport across the sediment-water interface. *Water Resources Research* 54(4): 2799–2812.
Voermans, J. J., Ghisalberti, M. & Ivey, G. N. 2018b. The Hydrodynamic Response of the Sediment-Water Interface to Coherent Turbulent Motions. *Geophysical Research Letters* 45(19): 10,520–10,527.
Vollmer, S., de los Santos Ramos, F., Daebel, H. & Kühn, G. 2002. Micro scale exchange processes between surface and subsurface water. *Journal of Hydrology* 269(1–2): 3–10.
Wohl, E. 2016. Spatial heterogeneity as a component of river geomorphic complexity. *Progress in Physical Geography* 40(4): 598–615.
Yang, J. Q., Chung, H. & Nepf, H. M. 2016. The onset of sediment transport in vegetated channels predicted by turbulent kinetic energy. *Geophysical Research Letters* 43(21): 11,261–11,268.
Yang, J. Q. & Nepf, H. M. 2018. A turbulence-based bed-load transport model for bare and vegetated channels. *Geophysical Research Letters* 45(19): 10,428–10,436.
Yang, J. Q. & Nepf, H. M. 2019. Impact of vegetation on bed load transport rate and bedform characteristics. *Water Resources Research* 55(7): 6109–6124.
Yuan, Y., Chen, X., Cardenas, M. B., Liu, X. & Chen, L. 2021. Hyporheic exchange driven by submerged rigid vegetation: a modeling study. *Water Resources Research* 57(6): e2019WR026675.